Available online at www.sciencedirect.com
ScienceDirect
Journal of Photochemistry and Photobiology A: Chemistry 190 (2007) 228–240
Journal of Photochemistry and Photobiology A:Chemistry
www.elsevier.com/locate/jphotochem

The on-the-fly surface-hopping program system NEWTON-X: Application to ab initio simulation of the nonadiabatic photodynamics of benchmark systems

Mario Barbatti [a,*], Giovanni Granucci [b,*], Maurizio Persico [b,*], Matthias Ruckenbauer [a], Mario Vazdar [c], Mirjana Eckert-Maksić [c], Hans Lischka [a,*]

[a] *Institute for Theoretical Chemistry, University of Vienna, Waehringerstrasse 17, 1090-Vienna, Austria*
[b] *Dipartimento di Chimica e Chimica Industriale, Università di Pisa, v.Risorgimento 35, 56126 Pisa, Italy*
[c] *Laboratory for Physical-Organic Chemistry, Division of Organic Chemistry and Biochemistry, Rudjer Bošković Institute, Zagreb, Croatia*

Received 23 October 2006; accepted 1 December 2006
Available online 15 December 2006

Abstract

The great importance of ultrafast phenomena in photochemistry and photobiology has made dynamics simulations an essential methodology in these areas. In this work, we present the NEWTON-X program package containing a new implementation of a direct dynamics approach to perform adiabatic (Born–Oppenheimer) and nonadiabatic simulations. The nonadiabatic dynamics is based on Tully's surface hopping approach. The program has been developed with the aim of (1) to create a flexible tool to be used in connection with a multitude of third-party electronic-structure program packages and (2) to provide the most common options for excited-state dynamics simulations. Benchmark calculations on the nonadiabatic dynamics are presented for the methaniminium, butatriene and pentadieniminium cations. The simulation of UV absorption spectra is presented for the methaniminium cation and pyrazine.

Keywords: Nonadiabatic phenomena; Excited state dynamics; Ultrafast photochemistry; On-the-fly surface-hopping dynamics; Ab initio dynamics

1. Introduction

In this paper we present computational methods and a new program system developed in our groups for the simulation of excited state dynamics. Illustrative examples are used to show the capabilities of the program. The method is based on a "direct" on-the-fly approach for the computation of classical trajectories with Tully surface hopping [1] using energy gradients and nonadiabatic coupling vectors calculated by means of available quantum chemical program systems. Ab initio direct calculations of excited state dynamics have been performed in recent years by several groups [2–16]. The increasing interest in this field warrants the introduction of standardized and flexible computational tools, available to the scientific community.

When choosing a method to simulate excited state molecular dynamics one faces three main issues: the first one is how to solve the fixed nuclei electronic problem, the second one is how to treat the nuclear dynamics and its coupling to the electronic dynamics, and the third issue is apparently a technicality, namely whether the computation of the potential energy surface (PES) should be dealt with beforehand or "on-the-fly". In fact, this choice is conditioned by the previous ones and by the processes to be investigated. The alternatives are to determine the PES and couplings systematically in advance and to represent them analytically for use in the simulations (two-step strategy), or to compute them at each time step during the integration of the dynamical equations as needed (direct or on-the-fly strategy). It should be stressed at this point that the calculation of electronically excited states, analytic energy gradients and nonadiabatic coupling vectors is still a formidable problem and only few specialized methods and quantum chemical program systems are available for that purpose.

In the two-step approach, the number of single point electronic structure calculations to be executed increases

* Corresponding author. Tel.: +43 1 4277 52757; fax: +43 1 4277 9527.
E-mail addresses: mario.barbatti@univie.ac.at (M. Barbatti), granucci@dcci.unipi.it (G. Granucci), mau@dcci.unipi.it (M. Persico), hans.lischka@univie.ac.at (H. Lischka).

1010-6030/$ – see front matter © 2006 Elsevier B.V. All rights reserved.
doi:10.1016/j.jphotochem.2006.12.008

exponentially with the dimensionality of the problem, i.e. with the number of nuclear degrees of freedom that are taken into consideration. As a consequence, the application of this strategy is severely restricted: a rigorous treatment is limited to small molecules (5–6 atoms), and for larger systems one must either select few internal coordinates and ignore the other ones, or resort to simplifying assumptions as to the form of the PES and couplings. The analytic representation of the electronic quantities can be rather involved, and its parameterization will be quite a cumbersome task if the PESs do cross and/or several reaction channels must be taken into account. The cusps of the PES and divergences of the derivative couplings can be dealt with by resorting to effective Hamiltonians in a quasi-diabatic representation [17,18] (see [19–21] for an application of this strategy to the photofragmentation of azomethane).

All these difficulties are avoided in the direct approach, which is therefore the most straightforward choice when several nuclear coordinates play non-trivial roles and the topology of the PES is complicated. In all kinds of trajectory calculations (two-step or direct), state energies, their gradients with respect to the nuclear coordinates, and the nonadiabatic couplings are required for the given geometry at each time step. In the direct approach, the number of single point calculations is $N_S \cdot N_T$, where N_S is the number of time steps and N_T the number of trajectories to be run. For a single trajectory, the computational cost does not depend on the number of internal coordinates (assuming the availability of proper analytic gradients and nonadiabatic coupling vectors) but is proportional to the propagation time, i.e. the time length of the process under investigation. Of course, the necessary number of trajectories will depend on the problem. In particular in the case of ultrafast processes only a small number of internal degrees of freedom will be relevant for the sampling process. This fact leads to a relatively small number of required trajectories. Thus, this approach is especially suited for the treatment of ultrafast processes, which require relatively short simulation times of a few ps. At this point we want to mention new approaches using interpolation techniques (see e.g. Ref. [22]) where the systematic computation of energy grids is avoided.

Because of the non-local character of quantum mechanics, in principle the direct approach cannot be applied to quantum wavepacket calculations and to adequately describe effects such as tunneling. However, by expanding the wavepackets on localized travelling basis functions and introducing suitable approximations, the direct approach becomes a viable alternative, although the computational cost of a method such as the full multiple spawning (FMS) [6] increases more than linearly with the propagation time. In fact, in the FMS procedure the number of electronic calculations per run and per time step is within the range $[N_b, N_b(N_b + 1)]$, where N_b is the number of travelling basis functions (increasing with time).

In this paper we shall describe computer software based on classical trajectories that are most conveniently connected with the direct calculation of electronic quantities. In particular, we have chosen Tully's surface hopping (SH) method [1,10,23–29], but other trajectory methods can be easily implemented, such as mean-field (MF) [30–34] or intermediate (SH–MF) [35] approaches.

The implementation of direct dynamics methods can be achieved in several ways. One possibility is to tie all program steps closely together into one homogeneous program package. This approach will give maximum computational efficiency. However, it will be strongly connected to a chosen quantum chemical program system providing the electronic energies and other data as discussed before. These quantum chemical program sections are the most complex and extended parts of the entire program. Usually, the quantum chemical calculation performed at each time step requires by far more computer time than the numerical integration steps of Newton's equations and the integration of the electronic Schrödinger equation along the trajectory. Thus, a modular approach appears to be more profitable. There, the computational steps of the time integration and the quantum chemical part are strictly separated, as described below. The big advantage of this modular approach is the fact that it is only loosely linked to a given quantum chemical program package. Since these quantum chemical program sections are always in rapid development, insertion of new features are easily achieved while keeping all remaining software environment unchanged. The disadvantage of this approach is the introduction of computational overhead, which is, however, relatively small compared to the large computer times of the quantum chemical calculation.

The program NEWTON-X [36] to be described in this publication has been developed in a joint effort along the concept of modularity. As will be described below, the creation of interfaces to the quantum chemical program section is straightforward allowing the use of the most suitable method available in each case.

2. Method

2.1. Dynamics implementation

In this section we give a short description of the standard classical trajectory surface hopping (TSH) procedure [1,10,27,37] that we have adopted in the NEWTON-X package, with emphasis on the options available to run ab initio on-the-fly dynamics. The nuclear motion is represented by classical trajectories, computed by numerical integration of Newton's equations by the velocity-Verlet algorithm [38,39]. The molecule is considered to be in a given electronic state (the current state) at any time. While the system is in the adiabatic state ψ_K the nuclear trajectory is driven by its PES, E_K. Imposing the electronic wavefunction (expanded in the basis of the first N_A adiabatic states) to obey the time-dependent Schrödinger equation, we get the following set of coupled differential equations for the probability amplitudes A_K:

$$\dot{A}_K(t) = -\sum_{L=1}^{N_A} A_L(t)\, e^{i\gamma_{KL}} \dot{\mathbf{Q}}\, \mathbf{h}_{KL}, \tag{1}$$

where $\hbar\gamma_{KL} = \int_0^t (E_K - E_L)\, dt'$, $\dot{\mathbf{Q}}$ is a vector collecting the nuclear velocities and $\mathbf{h}_{KL} = \langle \psi_L | \nabla_{\mathbf{Q}} \psi_K \rangle$ is the nonadiabatic coupling vector between states K and L. From the numerical integration of Eq. (1) the adiabatic populations $P_K(t) = |A_K(t)|^2$

are obtained. The transition probability to jump from one potential surface to another one is evaluated by looking at the variation of the $P_K(t)$'s in time on the basis of Tully's fewest switches algorithm [1,27,37] or alternatively using the modified fewest-switches algorithm proposed by Hammes–Schiffer and Tully [25].

Several integration schemes have been implemented in order to achieve high numerical stability together with time steps Δt as long as possible. Contrary to the adiabatic energies E_K, the nonadiabatic couplings, as function of the nuclear coordinates, can undergo rather abrupt variations and even diverge. For this reason, several algorithms have been provided for the integration of Eq. (1). The main ones are the 6th-order Adams–Moulton predictor-corrector scheme [40], the 5th-order Butcher method [41,42], and the unitary propagator $U(t, \Delta t)$:

$$A(t + \Delta t) \cong U(t, \Delta t)A(t), \tag{2}$$

$$U(t, \Delta t) = \exp\left(\frac{B(t) + B(t + \Delta t)}{2}\Delta t\right), \tag{3}$$

where B is the antihermitian matrix $B_{KL} = \exp(i\gamma_{KL})\mathbf{Q}\cdot\mathbf{h}_{KL}$.

The integrators implemented usually give similar results. However, with multiple crossings the norm-conserving unitary propagator is preferable. To further improve the numerical integration of the electronic time-dependent Schrödinger equation, a smaller timestep $\Delta t' = \Delta t/m_s$ can be used, with the relevant quantities $E_K(t)$, $\dot{\mathbf{Q}}(t)$ and $\mathbf{h}_{KL}(t)$ interpolated from t to $t + \Delta t$.

In previous work with semiempirical electronic wavefunctions, Granucci et al. [43] have implemented a different propagation algorithm, based on a local diabatization scheme, which is inherently stable even in the case of narrowly avoided crossings or in the proximity of conical intersections. We compared the performance of the Newton-X unitary scheme, based on the evaluation of the nonadiabatic couplings, with those of the local diabatization procedure, as implemented in a development version of the Mopac package [44]. The test case was a model neutral-ionic avoided crossing, and the semiempirical parameters were varied so as to change the position of the crossing point and the value of the electronic neutral-ionic coupling H_{12}. The results of the comparison are presented in Table ST1 (supplementary material). As one can see, the two schemes gave similar results. Only for very weakly avoided crossings, with transition probabilities greater than 95%, the diabatic algorithm was superior (i.e. it allowed the use of larger time steps).

In surface hopping dynamics the momentum has to be adjusted after the hopping in order to keep the total energy constant. In Newton-X it is possible to set this adjustment along the momentum direction, along the nonadiabatic coupling vector direction, or along the gradient difference vector direction. Another option refers to frustrated hopping (those hoppings that do not take place because there is no available kinetic energy to do that). The most common options are to keep the momentum or invert it. Both can be chosen in Newton-X.

The simulation of a photochemical or photophysical process requires the execution of a rather large number of trajectories (a "swarm"), in case of ab initio dynamics preferably of the order of 100 or more. All quantities of interest, such as quantum yields, state populations, energy disposal and transient spectra, are computed as averages over all trajectories. The number of trajectories to be run depends on the statistical uncertainty that can be accepted on the results, and on the probability of the relevant events. The program contains routines to control multiple trajectories and to perform the required statistical procedures (Fig. 1).

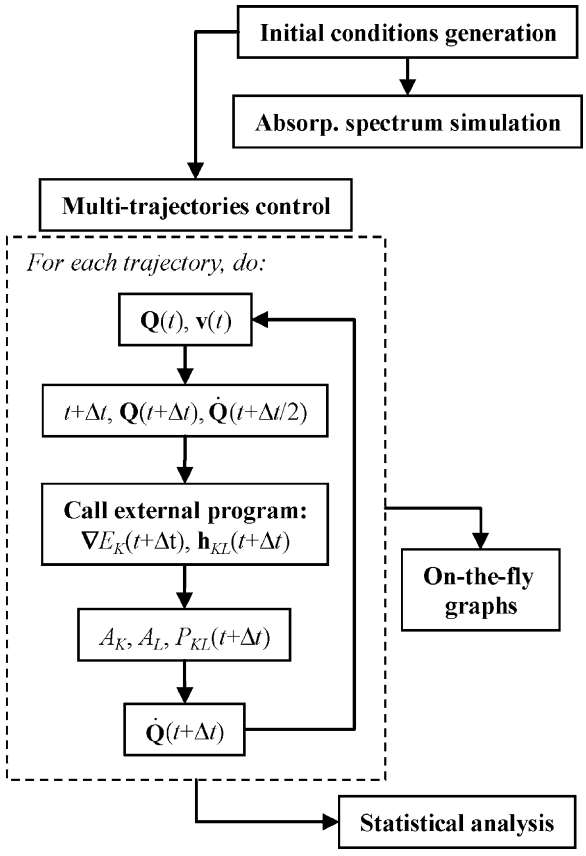

Fig. 1. Block structure of the Newton-X program.

As we have discussed in Section 1, Newton-X has been developed in a highly modular way, with several independent programs communicating via files. The main moduli are schematically shown in Fig. 1. At each integration timestep (Δt) of the Newton's equations, the electronic quantities E_K, $\nabla_Q E_K$ and $\mathbf{h}_{KL}$ have to be calculated (see Fig. 1) by some external program and provided to Newton-X. In principle, any ab initio program that could supply analytical energy gradients and eventually nonadiabatic couplings is eligible. For the time being, interfaces have been provided for the quantum chemistry packages Columbus [45–48], with which it is possible to perform nonadiabatic and adiabatic dynamics using SA–CASSCF (for the definition of acronyms see Section 2.3) and MR–CI methods; Turbomole [49] (adiabatic dynamics with RI–CC2 [50,51] and TD–DFT [52,53] methods); and the semiempirical package Mopac [44] (nonadiabatic dynamics). Presently, an interface to the Aces II package [54] is under development [55] allowing the performance of adiabatic and nonadiabatic dynamics using the EOM–CCSD method.

2.2. Initial conditions and absorption spectra

In NEWTON-X, the initial conditions (nuclear coordinates and momenta, and starting electronic state) are sampled so as to mimic at best a quantum wavepacket, and to take into account in a simplified way the excitation process. Coordinates and momenta are sampled according to their probability distributions in a given harmonic vibrational state. Harmonic frequencies and normal modes can be imported from the TURBOMOLE, GAMESS [56] and GAUSSIAN [57] packages. The sampling of coordinates and momenta can be either uncorrelated, i.e. they can be chosen by independent random events, or correlated. In the former case, the virial theorem $<E_{kin}>=<E_{pot}>$ is fulfilled, but the initial total energy is strongly dispersed. For the vibrational ground state, this initial conditions distribution matches the Wigner distribution for the quantum harmonic oscillator [58]. Alternatively, the sampling of coordinates and momenta can be correlated, which means that after sampling coordinates, the momenta are scaled to make the initial energy equal to the harmonic vibrational level (the zero point energy, if $v = 0$). This method, however, does not fulfill the virial theorem as it tends to overestimate the kinetic energy.

Some coordinates (normally the highest frequency ones) can be "frozen" in the sampling procedure, i.e. they can be fixed to equilibrium values with zero momenta: this may be useful, in order to reduce the total zero point energy and the artifacts connected with it (see for instance [59,60]).

For each molecular geometry that is selected by the sampling procedure, a stochastic algorithm can be executed to determine whether the trajectory will be started on the basis of the computed transition probability [61]:

$$P_{K0} = \frac{(f_{K0}/\Delta E_{K0}^2)}{\max(f_{K0}/\Delta E_{K0}^2)}, \quad (4)$$

where f_{K0} is the oscillator strength and ΔE_{K0} the energy gap. The probability is normalized by the maximum value of computed $f_{K0}/\Delta E_{K0}^2$ ratios. In this way, the effect of an ultrashort pulse is simulated, i.e. the creation of a "Franck–Condon" wavepacket in the excited electronic state without energy constraints. Note that this procedure is beyond the Condon approximation, as the oscillator strength is obtained for each molecular geometry. This feature can also be used to simulate the absorption spectrum, either by collecting in a histogram the number of accepted transitions as a function of the transition energy (histogram method) or by assigning to each transition a Gaussian function with the height P_{k0} and a width representing some phenomenological broadening and plotting the sum of these Gaussians as a function of the transition energy (Gaussian broadening method).

Additionally, the excitation can be restricted to a predefined energy window by imposing a constraint on the transition energy. In this case, instead of specifying the target excited state, one chooses the excitation energy E_X and a tolerance ΔE_X. Then, for each sampled geometry, the procedure considers the electronic states K for which the transition energy $E_K - E_0$ falls within the interval $E_X \pm \Delta E_X$ and starts a number of trajectories, distributed among those states, according to the probability defined in Eq. (4).

2.3. Computational details

Several electronic structure methods and levels of calculation have been employed for the photodynamical simulation of the systems methaniminium cation, butatriene, and pentadieniminium cations. Details on the methods and levels of calculation are summarized in Table ST2. Complete active space self-consistent field calculations with n electrons distributed in m orbitals (CASSCF(n, m)) have been performed on methaniminium, butatriene, and pentadieniminium cations, and on pyrazine. In all cases, a state averaging procedure has been used with equal weights for all k states involved (SA-k). In the case of the methaniminium cation, all configurations forming the CAS were used as references for subsequent multireference configuration interaction calculations with single and double excitations (MR–CISD). In the CI calculations the interacting space restriction [62] was applied and the 1s-core orbitals were kept frozen. In the case of the pentadieniminium cation, a subspace of the CAS(6,6) was used as reference for MR–CIS calculations. It is worth noting that MR–CIS is considerably more flexible than the conventional single reference CIS.

The time-dependent density functional theory (TD–DFT) and resolution-of-identity coupled-cluster method with double excitations (RI–CC2) have also been employed. The B3–LYP functional [63] was used in all TD–DFT calculations. Several (polarized) double-zeta quality basis sets have been used: 3-21G [64], 6–31G* [65], and SV(P) [66].

CASSCF and MR–CI gradients and nonadabatic coupling vectors were obtained with the analytical tools [67–70] implemented in the COLUMBUS program system. TD–DFT and RI–CC2 calculations were carried out with the TURBOMOLE package. Dynamics calculations have been performed with NEWTON-X.

3. Applications

Dynamics simulations have been performed for a series of systems, methaniminium cation, butatriene cation, and pentadieniminium cation (see Scheme 1). The photodynamics of all of these systems provide interesting challenges and questions and also may serve as benchmarks for testing new methods and programs. The methaniminium cation dynamics dependence on

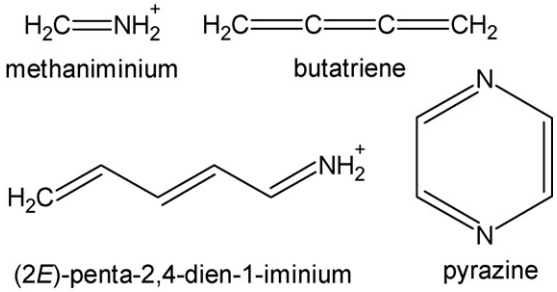

Scheme 1.

the initial surface is the subject of Section 3.1. The butatriene cation dynamics and the effect of the electronic structure calculation level and of the surface hopping algorithm are addressed in Section 3.2. The pentadieniminium cation dynamics dependence on the electronic structure method is discussed in Section 3.3. Furthermore (Section 3.4), simulations of the absorption spectra of methaniminium cation and pyrazine are presented. In Table ST2 (supplementary material) the main computational procedures used in each one of the dynamics simulations are summarized.

3.1. Methaniminium ($CH_2NH_2^+$) cation

The methaniminium has been studied as prototype for protonated Schiff bases [71], for polar π-bonds [16,72–74], and for basic processes of dehydrogenation [75–77]. Its small size and consequent reduced computational demands make methaniminium always a good candidate to test new methodologies [11,78].

Despite its apparent simplicity, the electronic structure of $CH_2NH_2^+$ shows an interesting complexity in terms of the $\sigma\pi^*$ (S_1) and $\pi\pi^*$ (S_2) states not present in the larger member of the PSB series $CH_2(CH)_kNH_2^+$ [79,80]. It has been found by Michl and Bonačić-Koutecký [72] that following the torsional motion, the $\pi\pi^*$ state is stabilized and crosses the S_0 state at 90°. Barbatti et al. [16] have shown that additionally the CN stretching mode is of great importance for the photodynamics since it is responsible for a crossing between the S_1 and S_2 states. Preliminary dynamics simulations demonstrated a strong sensitivity of the dynamics on the initial state. Starting in the $\pi\pi^*$ (S_2) state the dynamics was following the CN stretch and a simultaneous bipyramidalization of the CH_2 and NH_2 groups and not the torsional motion. The origin of this stretching seemed to be connected to the acquired momentum along the CN bond-direction during the initial motion on the S_2 surface before crossing to S_1. One interesting question not explored in the previous work was the point whether the torsion dominates the dynamics of the system excited into the S_1 state. The aim of the present work is a comprehensive simulation study of the S_1 and S_2 state dynamics of the methaniminium cation system using a much larger number of trajectories and the MR–CISD method instead of CASSCF.

As expected from the previous discussion, the results of the dynamics starting in the S_1 and S_2 states are qualitatively different. Trajectories starting in the S_1 state tend to present dominance of the torsional motion, without sign of CN dissociation. Fig. 2 shows the average fraction of trajectories in each state due to surface hopping as a function of time. As can be seen from Fig. 2b, during the first 10 fs, the time necessary for the system to rotate around the CN bond from 0° to 90°, there are virtually no hoppings. After this initial stage, the decay presents an exponential profile. The lifetime obtained from the average of 100 trajectories starting on S_1 is $\tau = 69 \pm 1$ fs. This lifetime was calculated from the exponential fitting with the function $f(t) = \exp(-t/\tau)$. Fig. 2 also shows the average adiabatic population (see Section 2.1) of state S_1. It matches quite well the average occupation of the state. This is a good indication of the quality of the surface hopping dynamics.

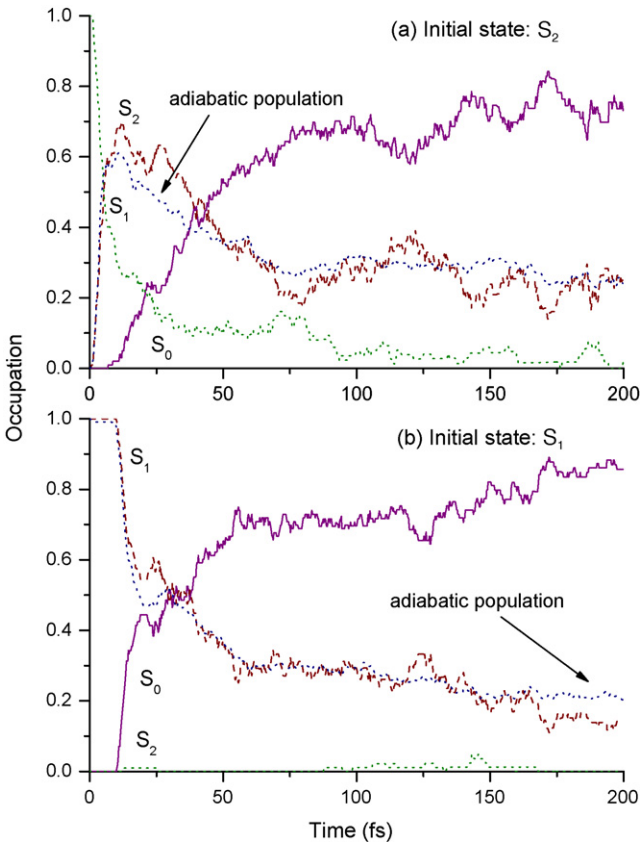

Fig. 2. Average fraction of trajectories for each state as function of time (fs) for the methaniminium cation. In (a), the initial state is S_2; in (b) the initial state is S_1. The average adiabatic population of state S_1 is also shown in each case.

When the dynamics starts in the S_2 state, this state is quickly depopulated in the first 10 fs while the occupation of the S_1 state increases to more than 60%, as shown in Fig. 2a. After about 15 fs, the ground state starts to be populated. The lifetime of the S_2 state (τ_2) is 12 ± 1 fs, similar to the 10 fs obtained previously at the CASSCF level [16]. The lifetime of the S_1 state (τ_1) is 65 ± 1 fs. It is given by the unimolecular decay model, by fitting the S_1 occupation with the function:

$$f(t) = \frac{\tau_1}{\tau_2 - \tau_1}\left[\exp\left(\frac{t}{\tau_2}\right) - \exp\left(\frac{t}{\tau_1}\right)\right]. \quad (5)$$

Fig. 3 shows the time evolution of the potential energy of the ground state and the excited states for three characteristic trajectories. As already mentioned before, the torsional motion dominates the S_1 dynamics. This feature implies a strong stabilization of the S_1 state during the first 10 fs (see Fig. 3c). In this particular trajectory, the system switches to the ground state, but returns to the excited state by means of a low-probability backhopping and finally decays to the ground state after 60 fs. Backhoppings occur often in the initial stage of the trajectories starting in S_1, reflecting on the one hand the periodicity of the torsional potential that recurrently brings the system close to a conical intersection and on the other hand the small number of internal coordinates, which limits the possibilities of energy flow.

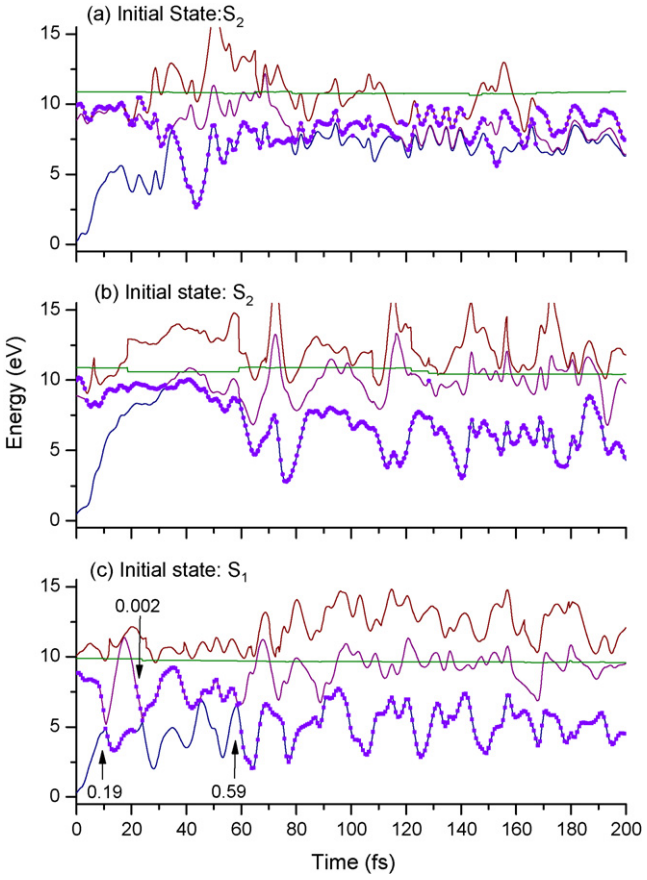

Fig. 3. Time evolution (fs) of the potential energy (eV) of the ground and excited states of the methaniminium cation in three qualitatively distinct trajectories. The dots indicate the current state of the system in each time step. In (a) trajectory type M and (b) trajectory type BP, the initial state is S_2; in (c) the initial state is S_1. The arrows in (c) show the probability of some hopping events.

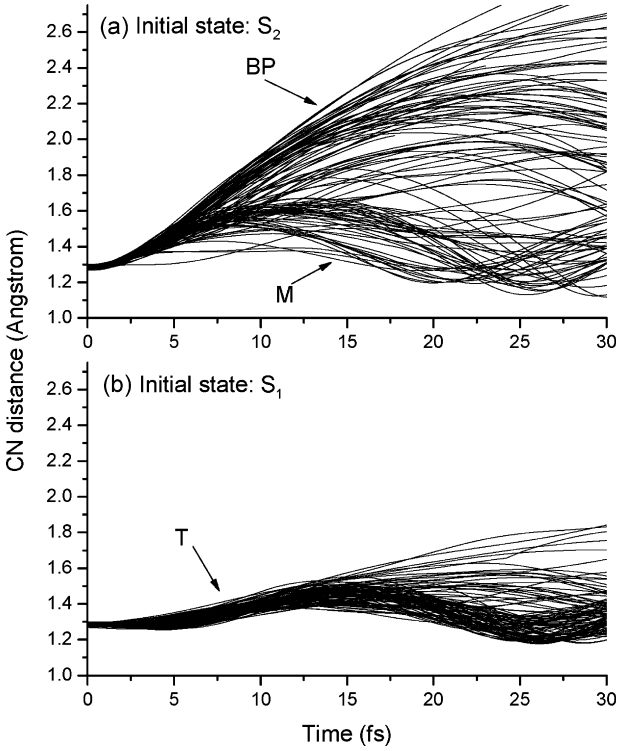

Fig. 4. Initial CN stretching (Å) of the methaniminium cation as function of time (fs) for trajectories starting in (a) S_2 and (b) S_1 states. The arrows indicate the three different types of trajectories: BP—bipyramidalization; T—torsion; M—mixed.

In case of trajectories starting in the S_2 state, more than one type of trajectories was observed. This can be seen from Fig. 4a in terms of the behavior of the CN distance. The main trunk of trajectories splits in two branches before 10 fs are reached. In the figure, they are indicated as BP (bipyramidalization) and M (mixed). Branch BP corresponds to the CN stretching mode with simultaneous bipyramidalization as described in Ref. [16] and represents about 50% of the total number of trajectories. A typical energy profile trajectory for type BP is shown in Fig. 3b. In this case the hopping to the ground state occurs at about 30 fs. Different from the torsional mode discussed before (Fig. 3c), the S_1 state is not stabilized along the BP trajectory. It is primarily the destabilization of the ground state that causes the S_1/S_0 crossing.

Trajectories of type M (Figs. 3 and 4a) constitute the other 50% of the total number of trajectories. They display a much more complicated motion that cannot be reduced to the dominance of any single internal coordinate such as torsion, CN stretch or bipyramidalization. Indeed, these trajectories behave like a mixing of the trajectories shown in Fig. 3b and c. The stretching motion is initiated exactly as in the BP trajectories. However, the CN distances only reach a maximum value of approximately 1.6 Å. The torsional motion is also initiated in the beginning of the simulation, but the pyramidalization of the CH_2 and NH_2 groups seems to inhibit the torsion, leading in summary to the aforementioned complicated mix of modes.

In trajectories of type M the CN stretching is reversed at relatively short distances (about 1.6 Å, as mentioned before), while in trajectories BP the CN stretching continues up to the much larger distance, giving origin to the $CH_2^+ \ldots NH_2$ complex at more than 2 Å. This indicates that the source of difference between the two types of trajectories could originate from an energetic barrier that is surmounted in the case of trajectories BP but not in the case of trajectories M. Trajectories at the bottom of branch M (Fig. 4a) of state S_2 have the same features in terms of energy profile, geometries and hoppings as trajectories of type T in state S_1 in Fig. 4b. This has led us to ask whether it is not possible to find trajectories of type M or even BP starting in the S_1 state. Inspection of trajectories shows that a small number of them may really be categorized as these other types rather than as type T.

The splitting of the trajectories in methaniminium is rather similar to the splitting observed in silaethylene (SiH_2CH_2) [81], involving even the same coordinates of torsion, bipyramidalization and stretching of the central bond. This suggests that the splitting can be a general feature of the dynamics of polar π-bonds.

The results of Ref. [16], obtained at the CASSCF level, do not allow the distinction between trajectories of types M and BP in a statistically significant sense since only 15 trajectories had been run previously. It is of great practical interest to know whether the splitting into two branches M and BP can also be

observed at the CASSCF level or whether it is a specific effect that depends on the MRCI energy surface. Therefore, we have run an additional set of 100 trajectories starting in the S_2 state using the SA-3-CAS(4,3)/6–31G* level. It was found that the trajectories also split in types M and BP similarly to those at MRCI level. Nevertheless, the lifetimes of the S_2 and S_1 states are 13 ± 1 and 43 ± 1 fs, respectively, while at MRCI level they are, as discussed above, 12 ± 1 and 65 ± 1 fs.

3.2. Butatriene ($C_4H_4^+$) cation

The photoelectron spectrum of butatriene (C_4H_4) shows two bands corresponding to the ionization of the π orbitals in- and out-of-plane [82]. Between these two bands appears a structured feature that has been explained in terms of the conical intersection between the $^2B_{2u}$ (D1) and the $^2B_{2g}$ (D_0) states of the butatriene cation ($C_4H_4^+$) [82,83]. Recently, wavepacket dynamics based on a five-dimensional model Hamiltonian and surface hopping calculations have been performed for the butatriene cation by Worth et al. [84]. The time evolution of the adiabatic population in the wavepacket dynamics shows two recurrence peaks at 40 fs and at 90 fs, which creates an oscillatory pattern in the D_1 population curve. Recently, Barbatti et al. [14] have observed that for ethylene similar oscillations in the adiabatic population predicted by wave packet dynamics [85] could be well described by surface hopping too. In the present work, we have investigated whether this is also true for butatriene cation.

We have performed surface hopping dynamics for the butatriene cation at the same electronic structure level (SA-2-CAS(5,6)/3–21G) as used in Ref. [84] to parameterize the analytical Hamiltonian and to perform the surface hopping dynamics. The present simulations were however carried out using somewhat different options than those employed in Ref. [84]. In our simulations the hopping was allowed for any energy gap, the CASSCF calculations were carried out with the state-average procedure for all points, and hoppings were allowed at any timestep, even immediately after another hopping. Besides that we have employed the fewest-switches algorithm to predict the hopping, while in Ref. [84] the hopping probability was assumed to be proportional to the adiabatic state population.

The general behavior of the adiabatic occupation of D_1 state in the present results is similar to the surface hopping results obtained in Ref. [84], including some repopulation of the D_1 state at 20 fs (see Fig. 5a). We found, however, an even slower decay of the adiabatic population, which comes closer to the wavepacket results of Ref. [83] than to those reported in Ref. [84].

We have also looked at the question whether the specific choice of the way of dealing with the momentum after a frustrated hopping has any influence on the results. One further set of 100 trajectory calculations (see Table ST2, $C_4H_4^+$, set 2) was carried out by inverting the momentum after a frustrated hopping. Although the results are essentially the same within the statistical uncertainty for the two cases, it seems that, based on the comparison of the position of the small recurrence peaks at about 50 fs with the wavepacket result, the procedure to keep the momentum gives slightly better results than to revert it. This conclusion is in line with the analysis of a similar problem by Müller and Stock [3].

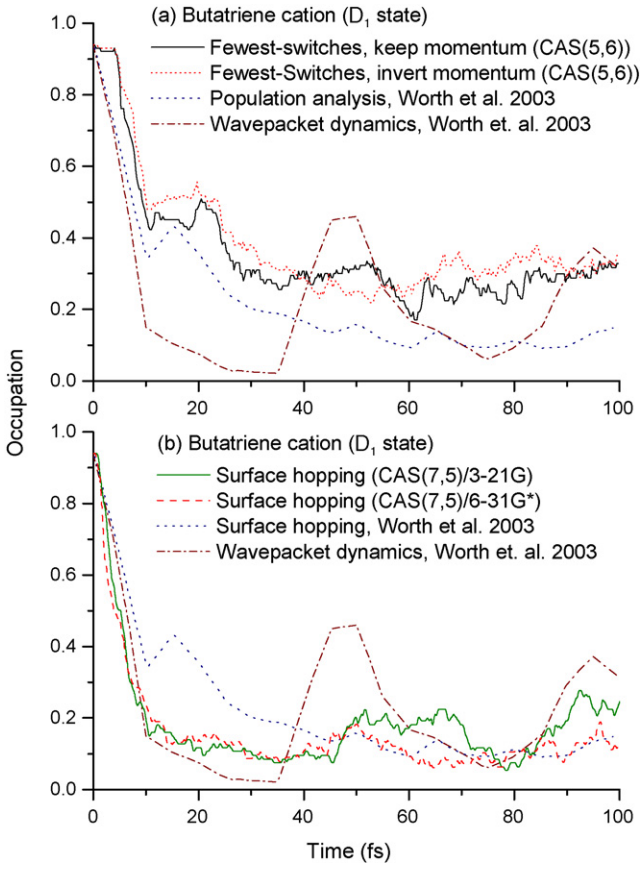

Fig. 5. Average fraction of trajectories for the butatriene cation in comparison with the wavepacket and surface hopping (population analysis) results of Ref. [84]. (a) CAS(5,6)/3–21G results inverting and keeping the momentum after a frustrated hopping; (b) CAS(7,5) results with 6–31G* and 3–21G basis sets.

The number of correlated electrons was increased as well in order to test the sensitivity of the dynamics on the computational level. Adopting an active space with 7 electrons distributed in 5 orbitals and using the 3–21 G basis set, the results look quite different (Table ST2, $C_4H_4^+$, set 3). In this case (Fig. 5b), the decay is much faster than with the CAS(5,6). The simulation also shows some oscillations in the adiabatic population, as can be seen in Fig. 5, although they are much less intense than those of the wavepacket dynamics.

A last set of 88 trajectory calculations was carried out using the same CAS(7,5) but now with the 6–31G* basis set (Table ST2, $C_4H_4^+$, set 4). Up to about 40 fs the results are essentially the same as those obtained with the 3–21 G basis set (Fig. 5b). After that, the oscillations with the 6–31G* basis set are more intense for the two peaks, although the first peak is shifted in time with respect to the wavepacket results.

We should also note that the Hamiltonian used in the wavepacket dynamics of Ref. [84] was parametrized by the CAS(6,5)/3–21G energy data. Therefore, we would not expect that any improvement in the ab initio level would result in the oscillations in the surface hopping dynamics. However, we have

seen that increasing the number of correlated electrons and of the basis set have this effect. This question should be further investigated using a higher quantum chemical level.

3.3. Pentadieniminium ($CH_2(CH)_4NH_2^+$) cation

The *all-trans*-pentadieniminium-cation (PSB3, a protonated Schiff-base with three double bonds) can be used as a first model for retinal, which is the central chromophore in the active center of the light-sensitive protein bacteriorhodopsin. Protonated Schiff-bases of different length (PSBn) have been intensively studied in the last years [7,8,80–90]. Based on minimum energy path investigations [86] and on dynamics simulations [7,8], Robb, Olivucci and co-workers have shown that the photoisomerization of PSBn can be described in terms of two states, S_0 and S_1, and two modes, the skeletal stretching and the torsional motion around a double bond.

In the present work, in addition to the selection of different multireference approaches and basis sets, we also chose two popular single reference methods (TD–DFT and RI–CC2) with the goal of testing their applicability for the photodynamics of retinal models. Although these single-reference methods cannot adequately describe the multireference states appearing in the regions of crossing, in some cases they could be conveniently used to describe the initial motion at low computational cost.

Five sets of trajectory calculations using different computational levels concerning the electronic structure calculation were performed. They are summarized in Table ST2. In the first step, SA-2-CASSCF(6,6) were performed. Based on these orbitals MR–CIS calculations were carried out using a CAS(4,5) reference wave function. Test calculations had shown that this reference space gave a good representation of the vertical excitation energies at a reduced computational cost. Two different basis sets (3–21 G and 6–31 G*) were used. Even though the 3–21 G basis is of very limited size, it is worth testing whether at least principal features of a dynamics can be reproduced with it since it is computationally much less demanding than the 6–31G* basis. Trajectory calculations using TD–DFT with the B3-LYP functional and the RI–CC2 method, in both cases with the SV(P) basis set, were also performed.

The occupation of the S_1 state of the MR–CIS and CASSCF trajectories (see Table ST2, PSB3, sets 1, 2 and 3 for a short characterization of the calculations) shows a delayed exponential decay, i.e. after remaining for a certain time in the excited state the occupation dropped exponentially from there on. In Fig. 6, the MR–CIS case is shown as a typical example. The lifetime was obtained by fitting the S_1 occupation with the function $f(t) = \exp((t - \tau_d)/\tau_e)$, where $f(t)$ is the fraction of trajectories and τ_d and τ_e are fitting parameters representing an initial delay and the time constant for the exponential decay, respectively. The overall lifetime, defined as the time necessary for the fraction of trajectories in the excited state to drop to 1/e is then the sum of τ_d and τ_e. The lifetimes obtained with different approaches are given in Table 1.

In agreement with the two-state two-mode model mentioned above, the results of the dynamics show that PSB3 begins to react to the excitation by elongating the double bonds and shortening the single bonds simultaneously. This behavior is described by the bond length alternation (BLA), which is defined as the difference between the averages of the single bond and double bond lengths, BLA = <*d*(single)> − <*d*(double)>. At the MR–CIS level (see Fig. 7a, left panel), the BLA begins at a small positive value of 0.025 Å, as given by the initial conditions, it drops within 30 fs to a negative value of about −0.1 Å and after 60 fs begins to increase again till it reaches its original value after 140 fs.

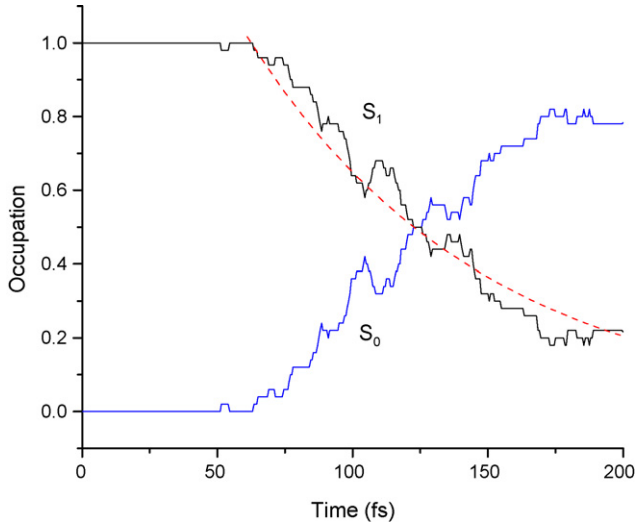

Fig. 6. Average fraction of trajectories on S_1 and S_0 states in function of time (fs) for PSB3 (MR–CIS level). The dashed line shows the exponential fitting.

In the process to reach the conical intersection the second main geometrical change in PSB3 occurs around the torsional angle of the central double bond, θ. This torsional angle has been shifted to the reference value 0° for the initial *trans* arrangement by defining $\theta = 180° - \omega$, where ω is the dihedral angle of the four carbons next to the central double bond. Starting from the *all-trans* geometry in the S_1 state, the molecule begins to twist around the double bond after a delay of roughly 50 fs, until the conical intersection is reached at a configuration close to 90° (Fig. 7a, right panel). The actual hoppings to the ground state are also indicated in this panel.

The average of $|\theta|$ at the point of the first hopping to the ground state (<$|\theta|$>) is 90° ± 5° at the MR–CIS level. The main features of the MR–CIS(4,5) trajectories are well reproduced by the CAS(6,6)/3–21G and CAS(6,6)/6–31G(d) simulations (see Table 1). However some differences can be observed. The onset of the S_1-state depopulation (Table 1) decreases and the distribution of the central torsional angle in the moment of hopping broadens with the decrease of the computational level. Moreover, at the CAS(6,6)/3–21G(p) level about 20% of the trajectories showed a torsion around the C=N bond without any central torsion at all, indicating that a secondary channel is being activated in this case. All these differences can be directly attributed to the excess of initial energy as given in the CASSCF method in comparison to the MRCI method (see vertical excitation energies in Table 1). Nevertheless, we should note that the lifetime and the average torsion angle at the first hopping (Table 1) are rather similar for the three methods.

Table 1
Vertical excitation energies (eV), averages of the absolute value of the central torsional angle (degrees) at the first hopping event, onset of the S_1-state depopulation (τ_d, in fs), and the lifetime ($\tau_d + \tau_e$, in fs) obtained from the dynamics simulation of PSB3

Level	E_{vert} (eV)	$<\|\theta\|>$ (degrees)	τ_d (fs)	Lifetime (fs)
MR–CIS(4,5)/3–21G	4.38	90 ± 5	62.5	149
SA-2-CASSCF(6,6)/6–31G*	4.76	92 ± 10	47.5	130
SA-2-CASSCF(6,6)/3–21G	4.85	91 ± 16[a]	32.5	153
TD–DFT(B3-LYP)/S V(P)	4.37	–	–	–
RI–CC2/SV(P)	4.39	–	–	–

[a] Including only the trajectories showing torsion around the central double bond.

The lack of nonadiabatic coupling vectors in TD–DFT and RI–CC2 methods restricts the calculations to an adiabatic dynamics, i.e. to a dynamics on the S_1 surface in this case. Unfortunately, the TD–DFT approach proved inadequate for the PSB3 simulation even in the beginning of the dynamics, as can be observed from the BLA behavior shown in Fig. 7b, left panel. Similar conclusions was already drawn from the static calculations of Refs. [80,87]. Moreover, a detailed analysis of the shortcomings of TD–DFT in this case has been given in Ref. [87]. Even more impressive is the complete lack of acti-

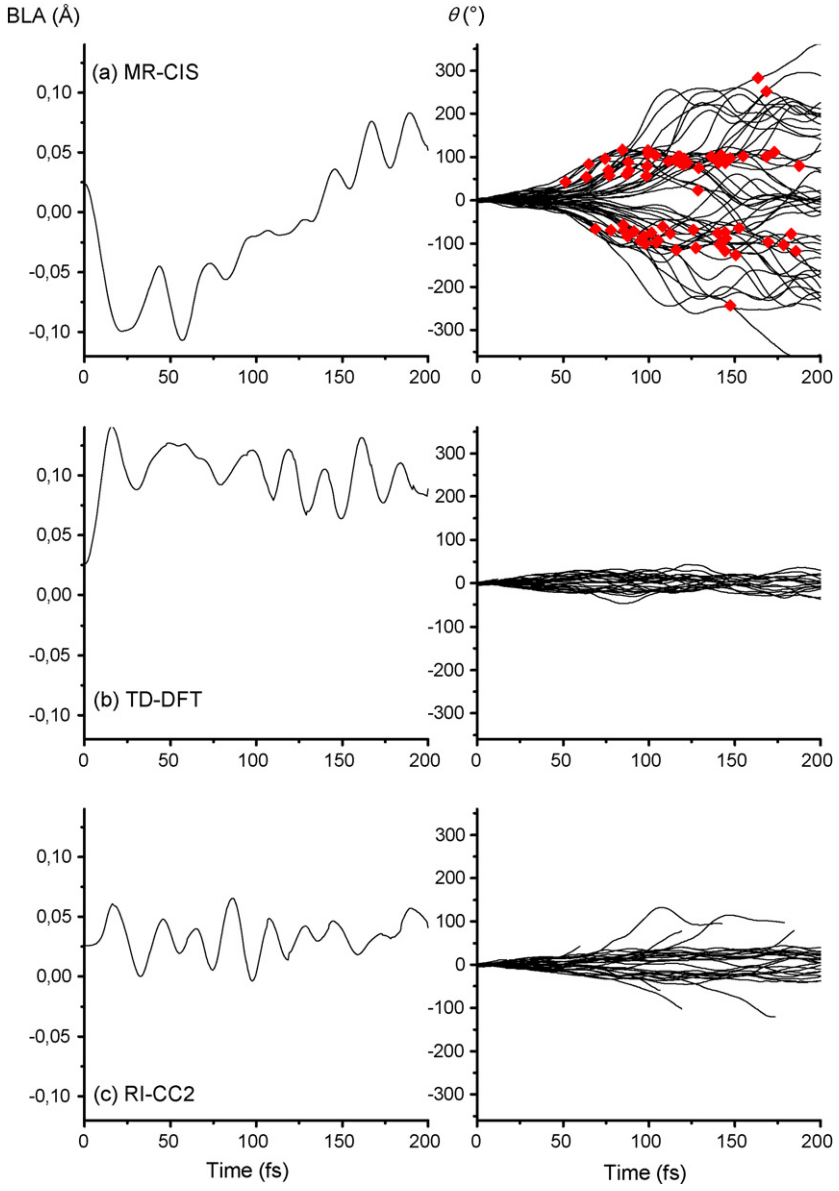

Fig. 7. Bond-length-alternation (BLA, in Å) and central torsion angle ($|\theta|$, in degrees) for PSB3 for each trajectory with (a) MR–CIS, (b) TD–DFT, and (c) RI–CC2. The diamonds in (a, right panel) indicate the first $S_1 \rightarrow S_0$ hopping events.

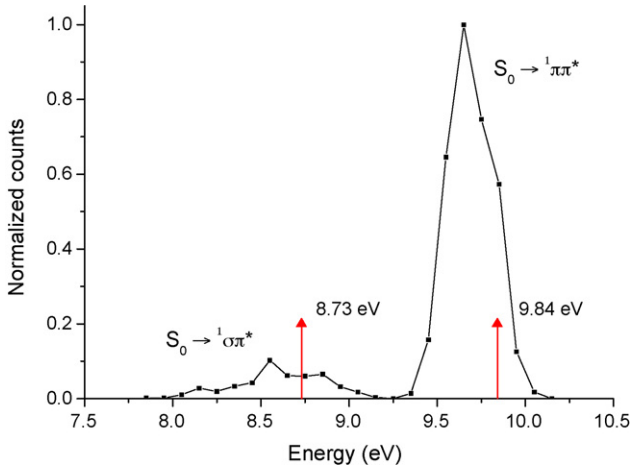

Fig. 8. Simulation of the absorption spectrum of the methaniminium cation using 4000 initial configurations (MRCI/SA-3-CAS(4,3)/6–31G*) and the histogram method. The arrows indicate the vertical excitation energies of the two peaks.

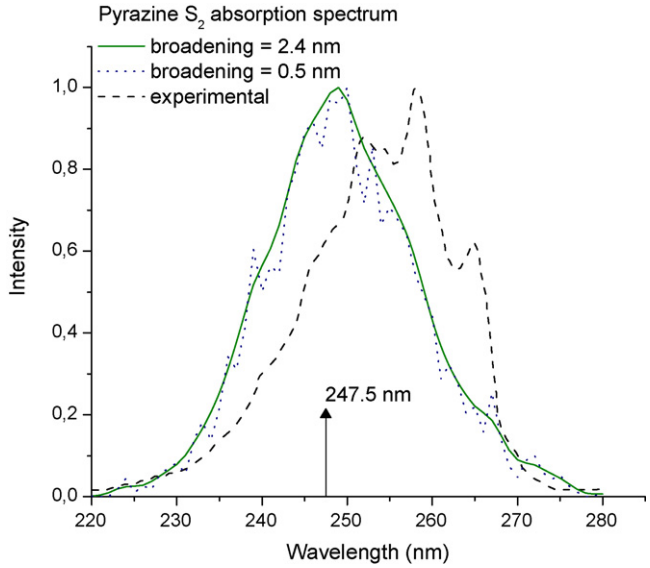

Fig. 9. Absorption spectrum of the S_2 state of pyrazine with two levels of Gaussian broadening. The experimental spectrum was taken from Ref. [82]. The arrow indicates the vertical excitation wavelength.

vation of the torsional motion, as one can see in Fig. 7b, right panel.

In the RI–CC2 calculations at least a few trajectories showed torsional motion (Fig. 7c, right panel). The BLA-changes however were described in a completely wrong way as well (see Fig. 7c, left panel). In Fig. 7c, right panel, it is also possible to see that the trajectories seem to be trapped around $|\theta| = 20^\circ$. This is an indication that the RI–CC2 S_1 surface contains a local minimum that is not present in the MR–CIS and CASSCF calculations.

3.4. Simulation of absorption spectra

In Section 2.2 we have outlined the procedures to simulate UV absorption spectra. Accurate simulations of UV spectra demand full quantum treatment and have been successfully performed for a variety of systems (see for example Ref. [82,91–97]). On the other hand, the present "semi-classical" simulation of an absorption spectrum has the advantage of being readily available and should be seen as a first approach to explain certain general features of a spectrum [98].

The absorption spectrum of the methaniminium cation shown in Fig. 8 has been computed from 4000 single point calculations at the MR–CISD/SA-3-CAS(4,3)/6–31G* level. The histogram method discussed in Section 2.2 with a bin size of 0.1 eV was used. Two points are worth noting. First, the vertical excitation energies are displaced to higher energies by about 0.2 eV in comparison to the corresponding peak maxima. This is a general effect that should be taken into account when comparing theoretical vertical transition energies and simulated or experimental spectra [99]. Second, the $S_0({}^1A_1) \rightarrow \sigma\pi^*({}^1A_2)$ transition is dipole forbidden at the C_{2v} minimum of ground state. The peak corresponding to this transition appears due to vibronic coupling. In the present approach this effect is taken into account due to the fact that the oscillator strength is calculated for initial geometries that are distorted to lower symmetry according to the quantum harmonic oscillator distribution resulting in a weakly allowed transition.

The simulation of the absorption spectrum for the S_2 ($\pi\pi^*$) state of pyrazine is shown in Fig. 9. It was computed from 2000 single point calculations at the SA-3-CAS(10,8)/6–31G* level, to which the Gaussian broadening method described in Section 2.2 was applied. Two spectra were generated with different Gaussian widths, 0.5 nm and 2.4 nm, representing the minimum and the maximal phenomenological broadening used in the simulations of Ref. [92].

Pyrazine has been intensively studied as an example of a dense spectrum resulting from a large number of states originated by vibronic coupling [82,91–94]. In particular, the band corresponding to the S_2-state absorption is broad and strongly perturbed by the interaction with the S_1 ($n\pi^*$) state, to which a fast relaxation takes place after the photoexcitation. The present simulation is able to reproduce the general shape of the $S_0 \rightarrow S_2$ band. The displacement of the band to shorter wavelengths can be attributed to the deficiencies of the CASSCF approach. The computed spectrum with broadening of 0.5 nm shows a fine structure, which is mostly related to statistical errors. Nevertheless, some of the peaks seem to be statistically relevant and also appear as shoulders in the spectrum using a broadening of 2.4 nm. Although one may be tempted to match these features with the experimental ones, further investigations are necessary in order to determine their origin.

4. Conclusions

The program system NEWTON-X has been presented, which allows the performance of direct surface-hopping dynamics calculations especially suited for the simulation of ultrafast photochemical processes. The special features of NEWTON-X are its modularity and the open approach for connecting to different quantum chemical program packages. Currently, the primary connections have been made to the program systems COLUMBUS,

TURBOMOLE and MOPAC. Incorporation of other program packages is straightforward. Connection to ACES II is in progress.

The set of benchmark examples consists of the methaniminium, butratriene and pentadieniminium cations, and pyrazine, for which dynamics and absorption spectra simulations were performed using several methods such as CASSCF, MR–CI, TD–DFT and RI–CC2.

The deactivation path of the methaniminium cation depended strongly on the fact whether the initially excited state was the $\sigma\pi^*$ (S_1) or the $\pi\pi^*$ (S_2) state. In the first case, the torsional motion dominates the photodynamics. The system deactivates through the region of the crossing seam that is reached at a torsional angle of 90°. When the dynamics starts in the S_2 state, two different types of trajectories can be observed: the first ones exhibit a mixing of torsion, CN-stretching and bipyramidalization, the second ones are characterized by simultaneous CN-stretching until close to dissociation and bipyramidalization but without any relevant torsional motion. The regions of the crossing seam where the nonadiabatic deactivation occurs are different in each case. Although MRCI and CASSCF results present the same features in terms of types of trajectories, the lifetime of the S_1 state is shorter at CASSCF level by more than 30%.

The effect of the specific choice of the parameters controlling the momentum after frustrated hoppings and of the electronic structure method was investigated in the dynamics of the butatriene cation. The main objective was to determine whether the surface hopping approach would be able to reproduce the strong oscillations in the adiabatic population as shown in the wavepacket dynamics. Such oscillations could be observed but were always much less intense than those resulting from the quantum treatment. However, it must be recalled that the quantum wavepacket calculations only considered five internal coordinates, limiting the vibrational energy transfer to other modes.

Dynamics calculations based on the CASSCF, MR–CIS, TD–DFT and RI–CC2 methods were performed for the pentadieniminium cation in order to test the influence of the electronic structure method and to search for possibilities to increase the computational efficiency. MR–CIS- and CASSCF-based dynamics confirms the two-states/two-modes model [86] proposed to explain the isomerization and deactivation of the protonated Schiff bases. In CASSCF dynamics the onset of the S_1-state depopulation occurs faster than in the MR–CIS case. When the 3–21G* basis set is used CASSCF also predicts the activation of a secondary isomerization path not present in MR–CIS results. These differences between CASSCF dynamics and MR–CI dynamics may mainly be attributed to the fact that the initial vertical excitation energy at CASSCF level is 0.5 eV higher than the initial energy at the MR–CI level.

The initial charge transfer character of the S_1 state and the multireference character of the problem at later stages of the isomerization process led TD–DFT to produce completely artificial results. Unfortunately, use of the RI–CC2 also did not improve the situation. However, it should be mentioned that in the case of excited-state proton transfer studies it has been shown that TD–DFT and RI–CC2 gave reliable results [100,101]. TD–DFT dynamics simulations on 2-(2′-hydroxyphenyl)benzothiazole and 10-hydroxybenzoquinoline have been carried out successfully in these cases [102].

NEWTON-X also allows the semiclassical simulation of absorption spectra, which was performed to the methaniminium cation and to pyrazine. The latter case presented good correspondence with available experimental spectra. The method can be regarded as a fast and straightforward first approach.

Acknowledgments

This work was supported by the Austrian Science Fund within the framework of the Special Research Program F16 (Advanced Light Sources) and Project P18411-N19. The authors are grateful for technical support and computer time at the Linux PC cluster Schrödinger III of the computer center of the University of Vienna. They acknowledge financial support by the WTZ treaty between Austria and Croatia (projects Nos. 9/2004 and 1/2006). The work in Zagreb (M.V. and M.E.-M.) was supported by the Ministry of Science Education and Sport of Croatia (Project No. 0098056). The work in Pisa was supported by the M.I.U.R. through the P.R.I.N. grant N0. 2004034838. This work was also sponsored by the COST D26 action, working groups 0014/03 and 0006/02.

Appendix A. Supplementary data

Supplementary data associated with this article can be found, in the online version, at doi:10.1016/j.jphotochem.2006.12.008.

References

[1] J.C. Tully, J. Chem. Phys. 93 (1990) 1061.
[2] T. Vreven, F. Bernardi, M. Garavelli, M. Olivucci, M.A. Robb, H.B. Schlegel, J. Am. Chem. Soc. 119 (1997) 12687.
[3] U. Müller, G. Stock, J. Chem. Phys. 107 (1997) 6230.
[4] A.L. Kaledin, K. Morokuma, J. Chem. Phys. 113 (2000) 5750.
[5] M. Hartmann, J. Pittner, V. Bonačić-Koutecký, J. Chem. Phys. 114 (2001) 2123.
[6] M. Ben-Nun, T.J. Martínez, Adv. Chem. Phys. 121 (2002) 439.
[7] O. Weingart, A. Migani, M. Olivucci, M.A. Robb, V. Buss, P. Hunt, J. Phys. Chem. A 108 (2004) 4685.
[8] C. Ciminelli, G. Granucci, M. Persico, Chem. Eur. J. 10 (2004) 2327.
[9] O. Weingart, V. Buss, M.A. Robb, Phase Trans. 78 (2005) 17.
[10] A.W. Jasper, D.G. Truhlar, J. Chem. Phys. 122 (2005) 044101.
[11] X. Li, J.C. Tully, H.B. Schlegel, M.J. Frisch, J. Chem. Phys. 123 (2005) 084106.
[12] C. Ciminelli, G. Granucci, M. Persico, J. Chem. Phys. 123 (2005) 174317.
[13] M. Barbatti, G. Granucci, M. Persico, H. Lischka, Chem. Phys. Lett. 401 (2005) 276.
[14] M. Barbatti, M. Ruckenbauer, H. Lischka, J. Chem. Phys. 122 (2005) 174307.
[15] R. Mitrić, V. Bonačić-Koutecký, J. Pittner, H. Lischka, J. Chem. Phys. 125 (2006) 024303.
[16] M. Barbatti, A.J.A. Aquino, H. Lischka, Mol. Phys. 104 (2006) 1053.
[17] T. Pacher, L.S. Cederbaum, H. Koppel, Adv. Chem. Phys. 84 (1993) 293.
[18] M. Persico, Electronic diabatic states: definition, computation and applications, in: P.v.R. Schleyer, N.L. Allinger, T. Clark, J. Gasteiger, P.A. Kollman, H.F. Schaefer III, P.R. Schreiner (Eds.), Encyclopedia of Computational Chemistry, Chichester, Wiley, 1998, p. 852.
[19] P. Cattaneo, M. Persico, Chem. Phys. Lett. 289 (1998) 160.

[20] P. Cattaneo, M. Persico, Theoret. Chem. Acc. 103 (2000) 390.
[21] P. Cattaneo, M. Persico, J. Am. Chem. Soc. 123 (2001) 7638.
[22] C.R. Evenhuis, X. Lin, D.H. Zhang, D. Yarkony, M.A. Collins, J. Chem. Phys. 123 (2005) 134110.
[23] R.K. Preston, J.C. Tully, J. Chem. Phys. 54 (1971) 4297.
[24] J.C. Tully, R.K. Preston, J. Chem. Phys. 55 (1971) 562.
[25] S. Hammes-Schiffer, J.C. Tully, J. Chem. Phys. 101 (1994) 4657.
[26] J.C. Tully, Faraday Discuss. 110 (1998) 407.
[27] D.S. Sholl, J.C. Tully, J. Chem. Phys. 109 (1998) 7702.
[28] J.-Y. Fang, S. Hammes-Schiffer, J. Phys. Chem. A 103 (1999) 9399.
[29] P.V. Parandekar, J.C. Tully, J. Chem. Phys. 122 (2005) 094102.
[30] M. Desouter-Lecomte, J.C. Leclerc, J.C. Lorquet, Chem. Phys. 9 (1975) 147.
[31] H.-D. Meyer, W.H. Miller, J. Phys. Chem. 70 (1979) 3214.
[32] G.D. Billing, Int. Rev. Phys. Chem. 13 (1994) 309.
[33] G. Stock, J. Chem. Phys. 103 (1995) 1561.
[34] X. Sun, W.H. Miller, J. Chem. Phys. 106 (1997) 6346.
[35] C. Zhu, S. Nangia, A.W. Jasper, D.G. Truhlar, J. Chem. Phys. 121 (2004) 7658.
[36] M. Barbatti, G. Granucci, H. Lischka, M. Persico, M. Ruckenbauer, Newton-X: a package for Newtonian dynamics close to the crossing seam, version 0.11b, www.univie.ac.at/newtonx, 2006.
[37] A. Ferretti, G. Granucci, A. Lami, M. Persico, G. Villani, J. Chem. Phys. 104 (1996) 5517.
[38] L. Verlet, Phys. Rev. 159 (1967) 98.
[39] W.C. Swope, H.C. Andersen, P.H. Berens, K.R. Wilson, J. Chem. Phys. 76 (1982) 37.
[40] D.L. Bunker, Meth. Comput. Phys. 10 (1971) 287.
[41] J. Butcher, J. Assoc. Comput. Mach. 12 (1965) 124.
[42] N.S. Bakhvalov, Numerical Methods, Mir publishers, Moscow, 1977, p. 495.
[43] G. Granucci, M. Persico, A. Toniolo, J. Chem. Phys. 114 (2001) 10608.
[44] J.J.P. Stewart, Mopac 2000 and Mopac 2002. Fujitsu Limited, Tokio, Japan.
[45] H. Lischka, R. Shepard, F.B. Brown, I. Shavitt, Int. J. Quant. Chem., Quant. Chem. Symp. 15 (1981) 91.
[46] R. Shepard, I. Shavitt, R.M. Pitzer, D.C. Comeau, M. Pepper, H. Lischka, P.G. Szalay, R. Ahlrichs, F.B. Brown, J. Zhao, Int. J. Quant. Chem., Quant. Chem. Symp. 22 (1988) 149.
[47] H. Lischka, R. Shepard, I. Shavitt, R.M. Pitzer, M. Dallos, Th. Müller, P.G. Szalay, F.B. Brown, R. Ahlrichs, H.J. Böhm, A. Chang, D.C. Comeau, R. Gdanitz, H. Dachsel, C. Ehrhardt, M. Ernzerhof, P. Höchtl, S. Irle, G. Kedziora, T. Kovar, V. Parasuk, M.J.M. Pepper, P. Scharf, H. Schiffer, M. Schindler, M. Schüler, M. Seth, E.A. Stahlberg, J.-G. Zhao, S. Yabushita, Z. Zhang, M. Barbatti, S. Matsika, M. Schuurmann, D.R. Yarkony, S.R. Brozell, E.V. Beck, J.-P. Blaudeau, Columbus, an ab initio electronic structure program, release 5.9.1 (2006, see http://www.univie.ac.at/columbus).
[48] H. Lischka, R. Shepard, R.M. Pitzer, I. Shavitt, M. Dallos, Th. Müller, P.G. Szalay, M. Seth, G.S. Kedziora, S. Yabushita, Z. Zhang, Phys. Chem. Chem. Phys. 3 (2001) 664.
[49] R. Ahlrichs, M. Bär, M. Häser, H. Horn, C. Kölmel, Chem. Phys. Letters 162 (1989) 165.
[50] A. Köhn, C. Hättig, J. Chem. Phys. 119 (2003) 5021.
[51] C. Hättig, J. Chem. Phys. 118 (2003) 7751.
[52] R. Bauernschmitt, R. Ahlrichs, Chem. Phys. Lett. 256 (1996) 454.
[53] F. Furche, R. Ahlrichs, J. Chem. Phys. 117 (2002) 7433.
[54] J. Gauss, J.D. Watts, W.J. Lauderdale, R.J. Bartlett, Int. J. Quant. Chem. Symp. 26 (1992) 879.
[55] A. Tajti, M. Barbatti, P. G. Szalay, H. Lischka, in preparation.
[56] M.W. Schmidt, K.K. Baldridge, J.A. Boatz, S.T. Elbert, M.S. Gordon, J.H. Jensen, S. Koseki, N. Matsunaga, K.A. Nguyen, S.J. Su, T.L. Windus, M. Dupuis, J.A. Montgomery, J. Comput. Chem. 14 (1993) 1347.
[57] M.J. Frisch, G.W. Trucks, H.B. Schlegel, G.E. Scuseria, M.A. Robb, J.R. Cheeseman, J.A. Montgomery Jr., T. Vreven, K.N. Kudin, J.C. Burant, J.M. Millam, S.S. Iyengar, J. Tomasi, V. Barone, B. Mennucci, M. Cossi, G. Scalmani, N. Rega, G.A. Petersson, H. Nakatsuji, M. Hada, M. Ehara, K. Toyota, R. Fukuda, J. Hasegawa, M. Ishida, T. Nakajima, Y. Honda, O. Kitao, H. Nakai, M. Klene, X. Li, J.E. Knox, H.P. Hratchian, J.B. Cross, V. Bakken, C. Adamo, J. Jaramillo, R. Gomperts, R.E. Stratmann, O. Yazyev, A.J. Austin, R. Cammi, C. Pomelli, J.W. Ochterski, P.Y. Ayala, K. Morokuma, G.A. Voth, P. Salvador, J.J. Dannenberg, V.G. Zakrzewski, S. Dapprich, A.D. Daniels, M.C. Strain, O. Farkas, D.K. Malick, A.D. Rabuck, K. Raghavachari, J.B. Foresman, J.V. Ortiz, Q. Cui, A.G. Baboul, S. Clifford, J. Cioslowski, B.B. Stefanov, G. Liu, A. Liashenko, P. Piskorz, I. Komaromi, R.L. Martin, D.J. Fox, T. Keith, M.A. Al-Laham, C.Y. Peng, A. Nanayakkara, M. Challacombe, P.M.W. Gill, B. Johnson, W. Chen, M.W. Wong, C. Gonzalez, J.A. Pople, Gaussian 03, Gaussian Inc., Wallingford CT, 2004.
[58] E. Wigner, Phys. Rev. 40 (1932) 749.
[59] R. Van Harrevelt, M. Van Hemert, J.C. Schatz, J. Chem. Phys. 116 (2002) 6002.
[60] D.M. Medvedev, S.K. Gray, E.M. Goldfield, M.J. Lakin, D. Troya, J.C. Schatz, J. Chem. Phys. 120 (2004) 1231.
[61] B.H. Bransden, C.J. Joachain, Physics of Atoms and Molecules, Longman, London and New York, 1983.
[62] A. Bunge, J. Chem. Phys. 53 (1970) 20.
[63] A.D. Becke, J. Chem. Phys. 98 (1993) 5648.
[64] J.S. Binkley, J.A. Pople, W.J. Hehre, J. Am. Chem. Soc 102 (1980) 939.
[65] W.J. Hehre, R. Ditchfield, J.A. Pople, J. Chem. Phys. 56 (1972) 2257.
[66] A. Schäfer, H. Horn, R. Ahlrichs, J. Chem. Phys. 97 (1992) 2571.
[67] R. Shepard, H. Lischka, P.G. Szalay, T. Kovar, M. Ernzerhof, J. Chem. Phys. 96 (1992) 2085.
[68] H. Lischka, M. Dallos, R. Shepard, Mol. Phys. 100 (2002) 1647.
[69] H. Lischka, M. Dallos, P.G. Szalay, D.R. Yarkony, R. Shepard, J. Chem. Phys. 120 (2004) 7322.
[70] M. Dallos, H. Lischka, R. Shepard, D.R. Yarkony, P.G. Szalay, J. Chem. Phys. 120 (2004) 7330.
[71] V. Bonačić-Koutecký, K. Schöffel, J. Michl, Theor. Chim. Acta 72 (1987) 459.
[72] J. Michl, V. Bonačić-Koutecký, Electronic Aspects of Organic Photochemistry, Wiley, New York, 1990.
[73] S. El-Taher, R.H. Hilal, T.A. Albright, Int. J. Quant. Chem. 82 (2001) 242.
[74] S. Zilberg, Y. Haas, Photochem. Photobiol. Sci. 2 (2003) 1256.
[75] K.F. Donchi, B.A. Rumpf, G.D. Willett, J.R. Christie, P.J. Derrick, J. Am. Chem. Soc. 110 (1998) 347.
[76] E. Uggerud, Mass Spectrom. Rev. 18 (1999) 285.
[77] T.H. Choi, S.T. Park, M.S. Kim, J. Chem. Phys. 114 (2001) 6051.
[78] S. Yamazaki, S. Kato, J. Chem. Phys. 123 (2005) 114510.
[79] P. Du, S.C. Racine, E.R. Davidson, J. Phys. Chem. 64 (1990) 3944.
[80] A.J.A. Aquino, M. Barbatti, H. Lischka, Chem. Phys. Chem. 7 (2006) 2089.
[81] G. Zechmann, M. Barbatti, H. Lischka, J. Pittner, V. Bonačić-Koutecký, Chem. Phys. Lett. 418 (2006) 377.
[82] G.A. Worth, L.S. Cederbaum, Annu. Rev. Phys. Chem. 55 (2004) 127.
[83] Chr. Cattarius, G.A. Worth, H.-D. Meyer, L.S. Cederbaum, J. Chem. Phys. 115 (2001) 2088.
[84] G.A. Worth, P. Hunt, M. Robb, J. Phys. Chem. A 107 (2003) 621.
[85] A. Viel, R.P. Krawczyk, U. Manthe, W. Domcke, J. Chem. Phys. 120 (2004) 11000.
[86] R. González-Luque, M. Garavelli, F. Bernardi, M. Merchán, M.A. Robb, M. Olivucci, Proc. Natl. Acad. Sci. U.S.A. 97 (2000) 9379.
[87] M. Wanko, M. Garavelli, F. Bernardi, T.A. Niehaus, T. Frauenheim, M. Elstner, J. Chem. Phys. 120 (2004) 1674.
[88] A. Cembran, F. Bernardi, M. Olivucci, M. Garavelli, J. Am. Chem. Soc. 126 (2004) 16018.
[89] J. Hufen, M. Sugihara, V. Buss, J. Phys. Chem. 108 (2004) 20419.
[90] M. Garavelli, Theor. Chem. Acc. 116 (2006) 87.
[91] T. Gerdts, U. Manthe, Chem. Phys. Lett. 295 (1998) 167.
[92] A. Raab, G.A. Worth, H.-D. Meyer, L.S. Cederbaum, J. Chem. Phys. 110 (1999) 936.
[93] M. Thoss, W.H. Miller, G. Stock, J. Chem. Phys. 112 (2000) 10282.
[94] D.V. Shalashilin, M.S. Child, J. Chem. Phys. 121 (2004) 3563.
[95] B. Schubert, H. Köppel, H. Lischka, J. Chem. Phys. 122 (2005) 184312.
[96] W.J.D. Beenken, H. Lischka, J. Chem. Phys. 123 (2005) 144311.

[97] A. Markmann, G.A. Worth, S. Mahapatra, H.-D. Meyer, H. Köppel, L.S. Cederbaum, J. Chem. Phys. 123 (2005) 204310.
[98] J.P. Bergsma, P.H. Berens, K.R. Wilson, D.R. Fredkin, E.J. Heller, J. Phys. Chem. 88 (1984) 612.
[99] Y.J. Bomble, K.W. Sattelmeyer, J.F. Stanton, J. Gauss, J. Chem. Phys. 121 (2004) 5236.
[100] A.L. Sobolewski, W. Domcke, Phys. Chem. Chem. Phys. 1 (1999) 3065.
[101] A.J.A. Aquino, H. Lischka, C. Hättig, J. Phys. Chem. A 109 (2005) 3201.
[102] R. de Vivie-Riedle, E. Riedle, A.J.A. Aquino, D. Tunega, M. Barbatti, H. Lischka, to be submitted for publication.